5. Shape of scoria cones on Mars: insights from numerical modeling of ballistic pathways

Petr Brož[1,2], Ondřej Čadek[3], Ernst Hauber[4] and Angelo Pio Rossi[5]

[1]Institute of Geophysics ASCR, v.v.i., Prague, Czech Republic

[2]Institute of Petrology and Structural Geology, Faculty of Science, Charles University, Prague, Czech Republic

[3] Department of Geophysics, Faculty of Mathematics and Physics, Charles University in Prague, Czech Republic

[4]Institute of Planetary Research, DLR, Berlin, Germany

[5]Jacobs University Bremen, Bremen, Germany

Status: Published in Earth and Planetary Science Letters 406,

doi:10.1016/j.epsl.2014.09.002.

5.0. Abstract

Morphological observations of scoria cones on Mars show that their cross-sectional shapes are different from those on Earth. Due to lower gravity and atmospheric pressure on Mars, particles are spread over a larger area than on Earth. Hence, erupted volumes are typically not large enough for the flank slopes to attain the angle of repose, in contrast to Earth where this is common. The distribution of ejected material forming scoria cones on Mars, therefore, is ruled mainly by ballistic distribution and not by redistribution of flank material by avalanching after the static angle of repose is reached. As a consequence, the flank slopes of the Martian scoria cones do not reach the critical angle of repose in spite of a large volume of ejected material. Therefore, the topography of scoria cones on Mars is governed mainly by ballistic distribution of ejected particles and is not influenced by redistribution of flank material by avalanching. The growth of a scoria cone can be studied numerically by tracking the ballistic trajectories and tracing the cumulative deposition of repeatedly ejected particles. We apply this approach to a specific volcanic field, Ulysses

Colles on Mars, and compare our numerical results with observations. The scoria cones in this region are not significantly affected by erosion and their morphological shape still preserves a record of physical conditions at the time of eruption. We demonstrate that the topography of these scoria cones can be rather well (with accuracy of ~10 m) reproduced provided that the ejection velocities are a factor of ~2 larger and the ejected particles are about ten times finer than typical on Earth, corresponding to a mean particle velocity of ~92 m/s and a real particle size of about 4 mm. This finding is in agreement with previous theoretical works that argued for larger magma fragmentation and higher ejection velocities on Mars than on Earth due to lower gravity and different environmental conditions.

5.1. Introduction and background

Until recently, the observational evidence of kilometer-scale edifices produced by explosive volcanic eruptions such as scoria cones, spatter cones, tuff cones and tuff rings on the martian surface was rare due to insufficient image resolution. On the other hand, theoretical predictions of their existence and relative importance had been developed in several studies (Wood, 1979; Dehn and Sheridan, 1990; Wilson and Head, 1994; Fagents and Wilson, 1996; Parfitt and Wilson, 2008). For a given erupted magma volume and volatile content, for example, considerable differences between pyroclastic cones on Earth and on Mars would be expected due to the different surface environment, in particular with respect to gravity and atmospheric pressure (e.g., Wilson and Head, 1994). Recent studies have expanded the known inventory of kilometer-scale volcanic edifices and have determined their morphologies (Bleacher et al., 2007; Keszthelyi et al., 2008; Meresse et al., 2008; Brož and Hauber, 2012, 2013). These studies revealed that scoria cones on Mars differ in morphology from those on Earth and display ~2.6 times larger basal diameters (Brož and Hauber, 2012).

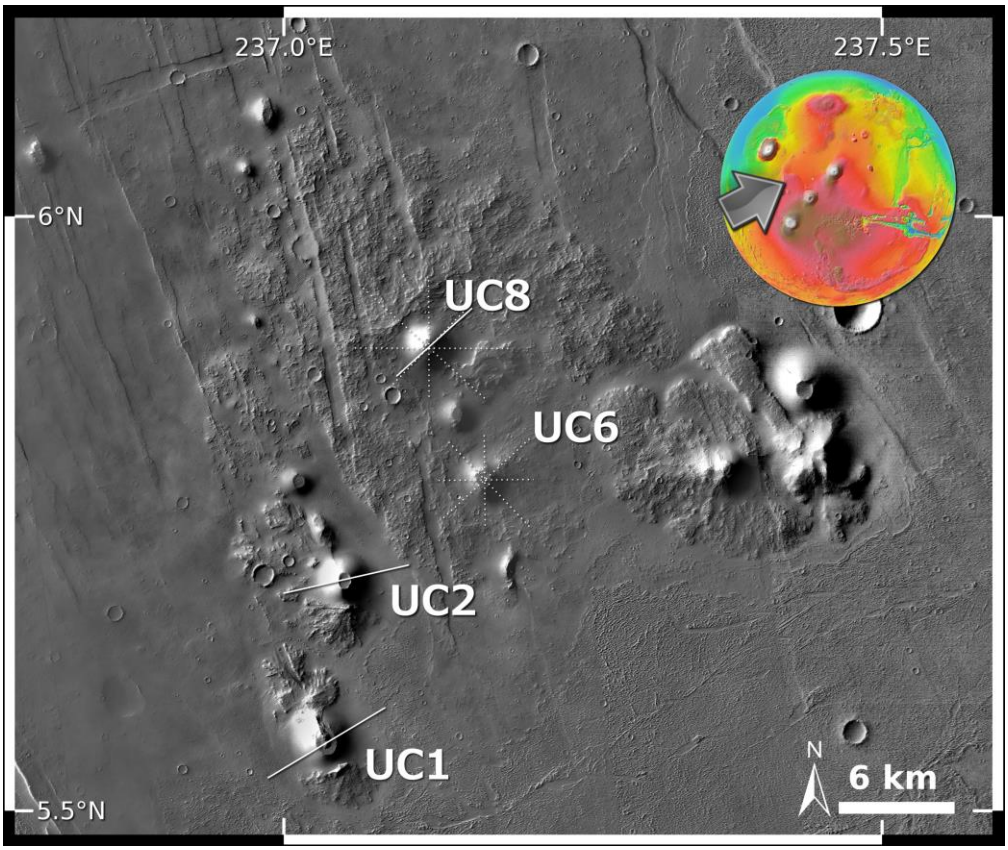

Fig. 5.1: Mosaic of CTX images covering Ulysses Colles in Tharsis on Mars. The field was described as volcanic in origin containing Martian equivalents to terrestrial scoria cones by Brož and Hauber (2012). Marked are cones used in this study with the position of HRSC DEM profiles (continuous lines) and CTX DEM profiles (dashed lines). Centered 5.8°N, 237.1°E, the mosaic of images number: CTX P19 008262 1862, P22 009554 1858 and G11 022582 1863.

Dehn and Sheridan (1990) modeled the shape of scoria cones on different terrestrial bodies (Mars, Earth and Moon) and predicted that, for a given magma volume, basal diameters (W_{CO}) of pyroclastic cones on Mars should be two to three times larger than on Earth. For a given eruption volume, the height (H_{CO}) of cones should be lower on Mars than on Earth because of the lower gravity and the resulting wider dispersal of particles (Wood, 1979). Wilson and Head (1994) estimated that for the same erupted volume the height of cones on Mars should be four times lower than on Earth, and central craters more than five times wider. Dehn and Sheridan (1990) suggest that martian cones should be more than 100 m

high and display well-developed central craters. Measurements of cones in the Ulysses Colles region (5.75°N, 237.1°E, Fig. 5.1), a volcanic field on Tharsis, showed that the average W_{CO} of the studied cones is ~2.6 times larger than for typical terrestrial scoria cones (Brož and Hauber, 2012), numerically corresponding with previously predicted values (Dehn and Sheridan, 1990). However, the martian cones are up to 650 m high, clearly contradicting the low heights predicted by Wood (1979b) and Wilson and Head (1994).

Scoria cones consist mainly of tephra particles that are produced via Strombolian eruptions by magma degassing and associated fragmentation (Parfitt and Wilson, 2008). Two main models exist to describe the exact mechanism of fragmentation (Jaupart and Vergniolle, 1989; Parfitt and Wilson, 2008), but both models predict the generation of a wide size range of pyroclasts that are ejected from a vent by explosive eruptions. Depending on particle size, tephra particles are transported away by two main processes. The finer particles are entrained in buoyant convective plumes and are transported far away from the vent by wind transport (Carey and Sparks, 1986; Wilson and Head, 1994; Kerber et al., 2013). The coarser size fractions (> ~1 cm) are mostly ejected on ballistic paths (Saunderson, 2008) close to the vent (Wilson and Head, 1994; Parfitt and Wilson, 2008), where they form a scoria cone. An alternative explanation of scoria cone formation, the jet fallout model, was proposed by Riedel et al. (2003). This model suggests that at least some parts of the cones grow by accumulation of clasts falling from an eruption jet column above the vent. Deposition by jet fallout was observed in situ at some scoria cones (Valentine et al., 2005) as partly contributing factor. Also, at least 50% of the ejected volume might be non-ballistically deposited around the cone as a thin ash blanket (Riedel et al., 2003), which would be hardly observable by remote sensing data in topographic profiles. The distribution of ballistically ejected material depends on particle size and density, initial velocity, the angle of ejection from the vent and the frequency of collisions between particles (Tsunematsu et al., 2014).

The final shape of the cone is controlled by the ballistic range of scoria particles and the total volume of generated scoria. This is only valid, however, until a critical volume of deposited material is reached, after which the cone flank attains the static angle of repose (~30°) and avalanching of tephra takes over as the main process determining the shape of the cone. The later redistribution is dependent on the maximum flank slope angle at which the material

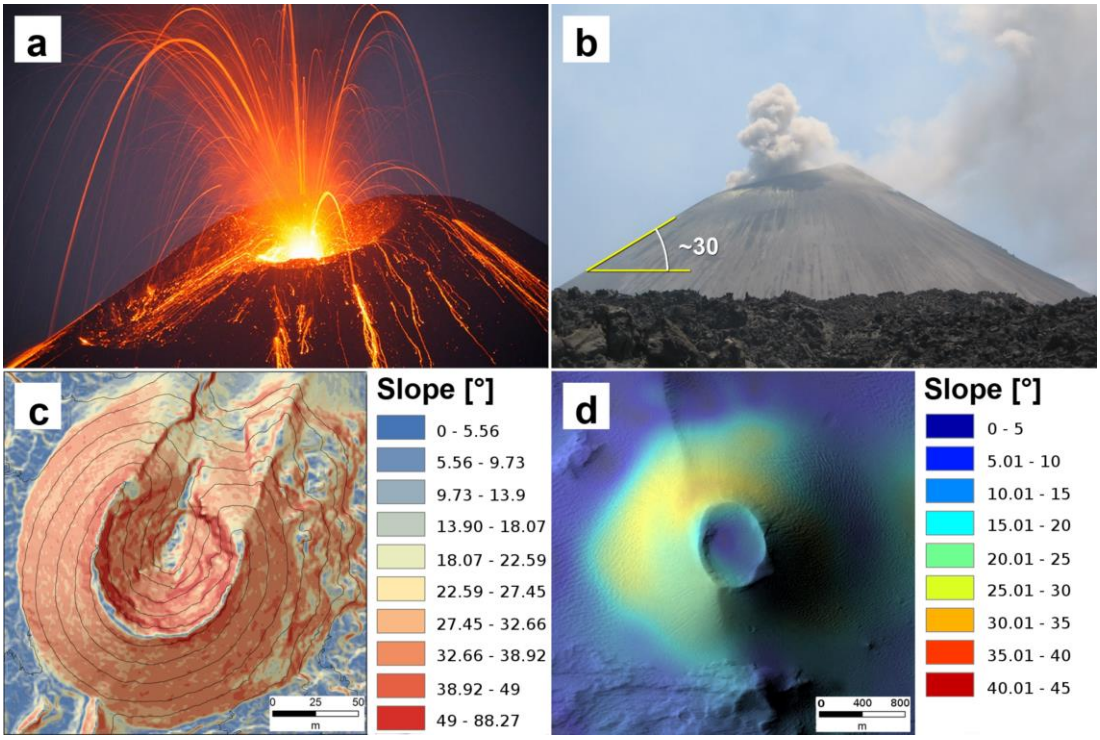

Figure 5.2: (a) Strombolian eruption at Anak Krakatoa, Indonesia in June 2009 (Image: Tom Pfeiffer). Note the ballistic trajectories highlighted in this evening photograph. (b) Scoria cone on Barren Island (Andaman Sea, India). The uniform flank slopes perfectly correspond to the angle of repose (~30°). Image courtesy of Hetu Sheth. (c) Slope map of Puu Kapanaha, a scoria cone at the eastern flank of Mauna Loa, Hawai`i (19.5474°N, 155.4557°W). Slopes were calculated on the basis of an airborne LIDAR-based Digital Elevation Model (DEM) (Hawaii Big Island Lidar Survey, doi: 10.5069/G9DZ067X; data provided by NCALM project, survey date 06/21/2009 - 06/27/2009). A best linear fit to the flank slopes yields 33°. Slopes increase to >40° very close to the summit, probably caused by spatter material that stabilizes the loose scoria particles. The black lines represent the counter lines with interval to be 5 m. (d) Cone UC 2 in the Ulysses Colles volcanic field. Slopes are derived from HRSC DEM. Background image is part of CTX image P22_009554_1858 (5.70°N, 237.04°E).

comes to rest, represented by the dynamic angle of repose (Riedel et al., 2003; Kleinhans et al., 2011). There is a debate whether the angle of repose is gravitationally dependent (Kleinhans et al., 2011) or not (Atwood-Stone and McEwen, 2013), however both studies confirm that the angle of repose for scoria material should be very similar for Earth and Mars.

Observations of martian scoria cones raise the question of why their shapes are so markedly different from scoria cones on Earth. This study focuses on this discrepancy, based on numerical modeling of tephra particle ejection and dispersion around the vent that builds on the work of several authors (e.g., McGetchin et al., 1974; Dehn and Sheridan, 1990; Riedel et al., 2003, Saunderson, 2008; Harris et al., 2012 and references therein). However, the present study adds to our understanding of scoria cone growth on Mars because (i) it point out the significance of larger dispersion of ejected material for the evolution of flank slopes (Fig. 5.2), (ii) compares modeling results with real morphologies of martian scoria cones, which was previously not possible, (iii) refines theoretical predictions about initial conditions in the time of explosive eruptions and (iv) shows predictions of the shape of martian scoria cones for different amounts of ejected material.

5.2. Data and methods

5.2.1. Numerical model

Scoria cones are built by clastic material ejected from the vent along ballistic trajectories. The final shape of the cone is given by the ballistic range of particles, depending mainly on ejection velocity, atmospheric drag and gravity acceleration, and by the subsequent redistribution of the material by avalanches, which occurs when the slope of the cone exceeds the angle of repose. The track of a particle can be reconstructed by numerical modeling (e.g., Riedel et al., 2003; Saunderson, 2006; Harris et al., 2012, and references therein; Tsunematsu et al., 2014). In the present study, we will deliberately construct our physical

model of cone growth as simply as possible to minimize the role of speculative parameters which are poorly understood even on Earth, let alone on Mars.

To a first approximation, the deceleration of the ejected particle due to atmospheric drag is given by (e.g., Parfitt and Wilson, 2008):

$$\boldsymbol{a_d} = -\frac{3}{4}\frac{C_d}{d}\frac{\rho_{air}}{\rho_{rock}}\, v\, \boldsymbol{v} \tag{5.1}$$

where $\boldsymbol{v}$ is the particle velocity vector, v is its magnitude, C_d is the drag coefficient, d is the particle size, and ρ_air and ρ_rock are the density of the air and the particle, respectively. The drag coefficient, $C_\mathrm{d,}$ depends on the shape, orientation and roughness of the particle and varies with the Reynolds (*Re*) and Mach (*M*) numbers. For a spherical particle, low *M*, and *Re* between about 300 and 2×10^5, C_d is nearly constant (≈ 0.5; Bird et al., 1960). This range of *Re* corresponds well to recent conditions on Mars, provided that $d \gtrsim 0.01$ m and $v \gtrsim 30$ m/s. The drag coefficients for realistic volcanic fragments are usually between the values for spheres and cubes (Alatorre-Ibargüengoitia and Delgado-Granados, 2006). In this study, we use $C_\mathrm{d} = 0.7$. The atmospheric density ρ_air of 0.01 kg/m^3 is chosen to correspond to the present-day conditions on Mars and is corrected for the altitude of Ulysses Colles situated ~4.5 km above the martian datum (Brož and Hauber, 2012). The ejected material is assumed to have a uniform density ρ_rock of 850 kg/m^3 (Lautze and Houghton, 2005; Harris et al., 2012).

It should be noted that for a given value of velocity v, the atmospheric drag is given by a combination of four parameters, C_d, d, ρ_{air} and ρ_{rock}. While parameters C_d and ρ_{rock} are rather well determined and their variations can affect the estimate of atmospheric drag by tens of percent at most, the values of the other two parameters, ρ_{air} and d, are rather uncertain and can vary by orders of magnitude. The particle size on Mars can significantly differ from the values observed on Earth (Wilson and Head, 1994), and the density of air at the time

of volcanic activity could be higher than at present. Moreover, there is a trade-off between the two parameters: the ballistic trajectory does not depend on the individual values of ρ_{air} and d, but only on their ratio. That is why, in this study, we keep the values of parameters ρ_{rock}, C_d and ρ_{air} constant and we only vary the particle size and the initial velocity. The results which we present below for the particle size can then be arbitrarily reinterpreted in terms of the other parameters.

In calculating the ballistic trajectories, we neglect the interaction between particles during the ballistic flight (Vanderkluysen et al., 2012; Tsunematsu et al., 2014) and we do not take into account the effect of drag reduction near the vent (Fagents and Wilson, 1993). Both effects are difficult to quantify under martian conditions and are probably of only minor importance. We have investigated the impact of the latter effect numerically and found only a small (<10%) difference between the cases with and without the reduced drag if the radius of the domain where the drag is significantly reduced was smaller than 500 m. This is in agreement with an estimate based on eq. (5) in Fagents and Wilson (1993) if we take into account that the clast range observed in the Ulysses Colles region is ~1500 m or larger.

The statistical distribution of size and initial (ejection) velocity of pyroclastic particles on Mars is not known. Using the data obtained during normal explosions at Stromboli, Harris et al. (2012) showed that these two quantities are only weakly correlated (see their Fig. 10) and questioned the traditional view that the ejection velocity linearly decreases with the square root of the particle size (Steinberg and Babenko, 1978). Harris et al. (2012) suggest that the relationship between these quantities is more complex and involves also other parameters, namely gas density and gas jet velocity, which significantly vary during th volcanic event and thus cannot be used as constant parameters. For simplicity and to avoid over-parameterization, we assume in the present study that the ejection velocity does not

depend on the particle diameter and each of the two quantities can be independently described by a log-normal probability distribution,

$$p(x) = const\ exp\ [-\frac{[log_{10}(x)-log_{10}(\mu)]^2}{2\sigma^2}] \quad (5.2)$$

where x is the variable, and $\log_{10}(\mu)$ and σ denote the mean and the standard deviation, respectively. The values of μ and σ are chosen so that the probability functions roughly fit the experimental data obtained for Stromboli by Harris et al. (2012). The mean size of particles is μ = 0.04 m with a standard deviation σ = 0.3 (cf. Fig. 9a in Harris et al., 2012). The log-normal distribution of ejection velocity is characterized by μ = 46 m/s and σ = 0.2 (cf. Table 3 in Harris et al., 2012). Only particles with sizes smaller than 0.3 m and ejection velocities between 10-300 m/s are considered. Besides this 'reference model', we also test ejection velocities which are up to three times larger and particle sizes which are up to 100 times smaller than in the reference model. This choice is motivated by the predictions made by Wilson and Head (1994) who argued for larger magma fragmentation due to the lower surface atmospheric pressure. In the result section, the values of ejection velocity and particle size will often be presented in a normalized form, related to the reference model. For example, the normalized velocity of 2 means that the value of μ in eq. (5.2) is chosen to be 92 m/s, thus two times larger than in the reference model. For the statistical distribution of ejection angles, $p(\alpha)$, we consider two set-ups, both showing a Gaussian distribution on a cross-section through the center of the cone,

$$p(\alpha) = const\ exp\ (-\frac{\alpha^2}{2\sigma^2{}_\alpha}) \quad (5.3)$$

but differing with respect to the parameter σ_α. The first set-up with σ_α=15.5° (hereinafter referred to as ECN – 'Ejection Cone – Narrow') roughly corresponds to a normal Strombolian erruption as observed by Gouhier and Donnadieu (2010), while the other set-up (σ_α=31°,

denoted by the abbreviation ECW – 'Ejection Cone – Wide') reflects the possibility that dispersion of ejection angles may be wider on terrestrial bodies with low atmospheric pressures than on Earth (Glaze and Bologa, 2000; Wilson and Head, 2007). In both cases, only the ejection angles smaller than 45º are considered.

In calculating the shape of the cone for a given set of model parameters, we assume that each ejected particle is stored at the place where it lands, and its distance from the center of the cone is fully determined by its ballistic trajectory and the current topography of the cone. The vertical coordinate of the ejection point as well as of the spot where the ejected particle hits the surface is gradually modified, in agreement with the growth of the cone. No redistribution by avalanches is considered. The particle ejection stops when the model height reaches the real height of the observed cone at the Ulysses Colles volcanic field. Therefore, the model is not limited by the volume of erupted particles – the volume increases continuously as needed to reach the required height.

The topographic height h of the cone at a point at distance r from the center can be computed as the total volume of the material stored in annulus with radii $r - \Delta r/2$ and $r + \Delta r/2$ divided by the area S of the annulus, $S = 2\pi r\Delta r$. If the particles are approximately spherical, we obtain,

$$h(r) = \frac{c_s}{12r\Delta r} = \frac{const}{r} \sum_i d_i^3 \qquad (5.4)$$

where d_i denotes the size of individual particles stored in the annulus. The coefficient c_s characterizes the storage properties of clastic material and generally depends on the shape of particles, their statistical distribution and the total height of the stored material. For simplicity, we assume c_s to be a constant in our study. The total number of particles used in predicting the shape of one cone is ~10^7 and Δr is chosen to be 10 m.

Table 5.1: Key parameters used for modeling of scoria cones on Mars.

Parameter	Earth	Mars	Comment
Drag coefficient	0.5 to 1 with a mean value of ~0.7 for scoria particles	0.7	The average terrestrial value is used due to a lack of in situ data.
Atmospheric density [kg/m^3]	1.2	0.01	Martian value corrected for altitude of 4500 m (position of Ulysses Colles).
Rock density [kg/m^3]	700 to 1000	850	The average terrestrial value is used due to a lack of in situ data (Lautze and Houghton, 2005; Harris et al., 2012).
Gravity [m/s^2]	9.81	3.71	
Initial velocity	log-normal distribution with a peak at 46 m/s	increased by a factor of 1-3	Terrestrial distribution is based on observation by Harris et al. (2012). Due to lower atmospheric density and resulting larger gas expansion, initial ejection velocities are expected higher on Mars than on Earth (Wilson and Head, 1994).
Particles size	log-normal distribution with a peak at 4 cm	decreased by a factor of 1-100	Distribution based on Harris et al. (2012). A higher degree of magma fragmentation is expected on Mars due to the lower atmospheric pressure (Wilson and Head, 1994).
Angle of repose	30°-33°	~30°	Kleinhans et al. (2011), Atwood-Stone and McEwen et al. (2013)
Ejection angles	Narrow ejection cone (see eq. 5.3. for details)	Wide ejection cone (see eq. 5.3. for details)	Gouhier and Donnadieu (2010), Glaze and Bologa (2000), Wilson and Head, (2007)

5.2.2. Topographic data

The topographic profiles of three cones in Ulysses Colles (UC1, UC2 and UC8) were determined from HRSC stereo images (Jaumann et al., 2007) and derived gridded digital

elevation models (DEM). HRSC DEM are interpolated from 3D points with an average intersection error of 12.6 m and have a regular grid spacing of 50 to 100 m (Gwinner et al., 2010). In the case of cones UC6 and UC8, additional CTX DEM were used to test the precision of HRSC DEM for kilometer-scale edifices. High-resolution topographic data were based on CTX stereo-derived DEM, which were computed from CTX stereo pairs (Malin et al., 2007) using the methods described, e.g., in Moratto et al. (2010). CTX DEM reach a spatial resolution of ~10 m/pixel and the vertical accuracy of the stereo-derived CTX DEM can be roughly estimated to be around few meters.

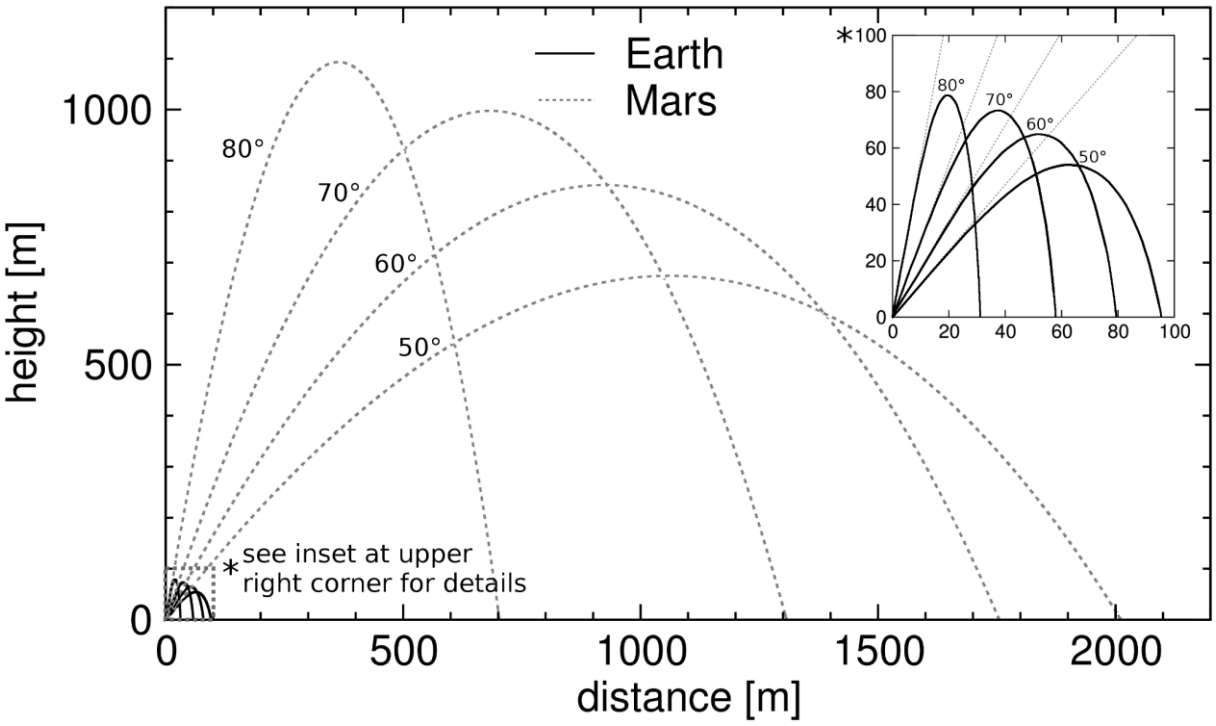

Figure 5.3: Ballistic pathways calculated for 4 cm-diameter particles with a density of 850 kg/m^3, ejected with velocities of 100 m/s at different ejection angles under present Martian (dashed lines) and terrestrial (black lines) environmental conditions (see Tab. 5.1). Note the significant differences in the transport distance between the planets.

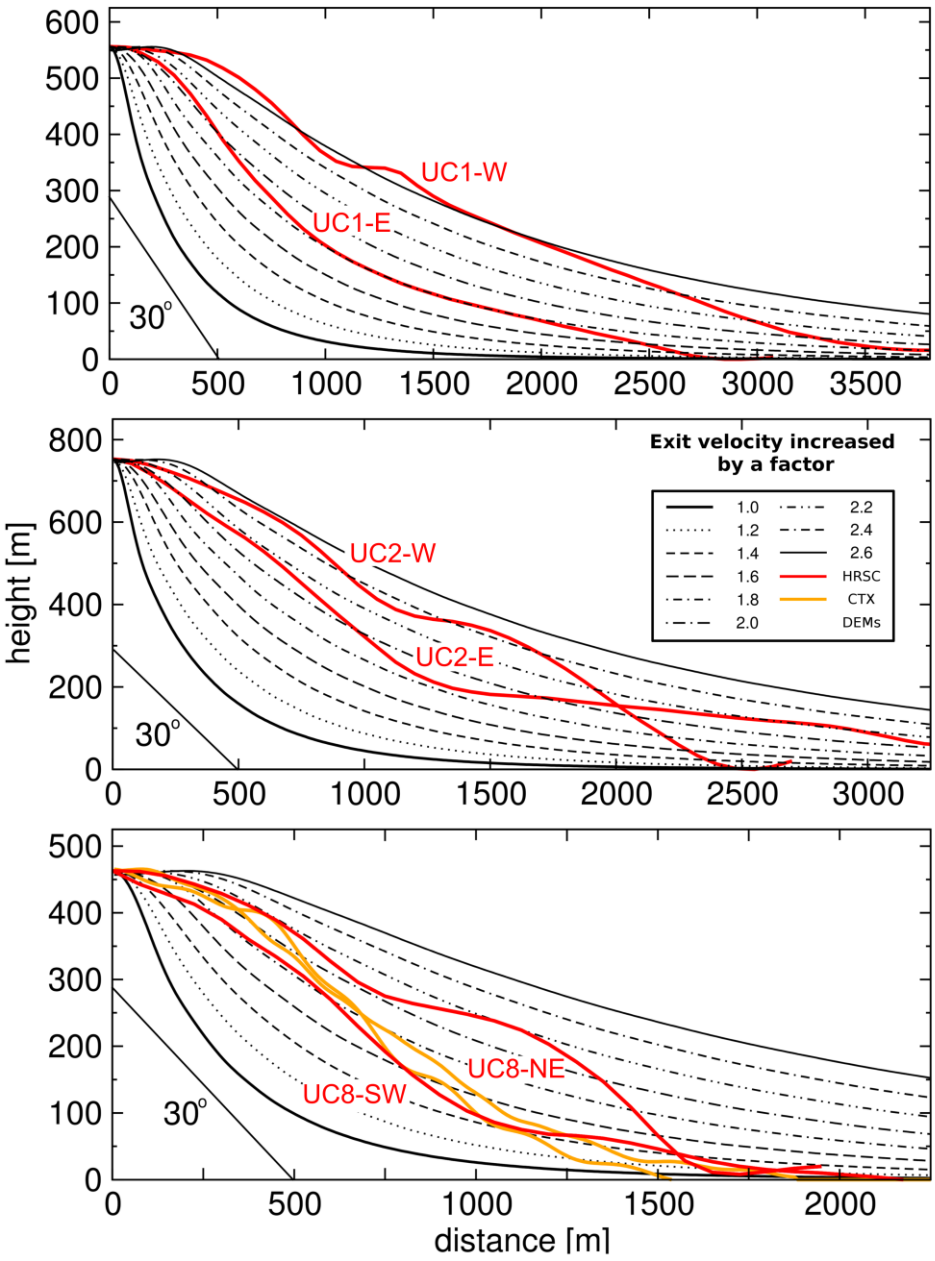

Figure 5.4: Comparison of the observed topographic profiles (HRSC data in red, CTX data in orange) of Martian cones in the Ulysses Colles region (upper panel: cone UC1, middle panel: cone UC2 and lower panel: cone UC 8, see Fig. 5.1 for the position of these cones) with the profiles of the same height computed for different ejection velocities (black lines) in the ECW set-up. If typical Earth-like ejection velocities are used in the current Martian environment (bold solid black line), the resulting shape is inconsistent with the observations. To reproduce the observed shapes, the initial ejection velocities must be increased (dashed lines). The relative (i.e. point-to-point) topographic errors are small as compared to the overall profile shape and are not taken into account. The best fit is obtained for initial velocities that are about two times larger than on Earth, in agreement with the theoretical prediction by Wilson and Head (1994). In all simulations, a particle size distribution (eq. 5.2) with μ = 4 cm is considered.

5.3. Results

A comparison of ballistic curves on Mars and Earth (Fig. 5.3) reveals that the maximum distance of ballistic transport is much larger on Mars than on Earth. While a 4 cm-particle ejected with an initial velocity of 100 m/s travels on Earth less than 100 m from the vent, the same particle reaches a distance of 2 km on Mars, thus about 20 times further. This difference is related to the lower values of atmospheric density and gravitational acceleration on Mars than on Earth (cf. Wood, 1979; Dehn and Sheridan, 1990; Wilson and Head, 1994). The ejected material is dispersed on Mars over a much larger area than on Earth which explains why the scoria cones observed on Mars are so wide, with a mean basal diameter of 1,500 m for cones in Hydraotes Chaos (Meresse et al., 2008) and 2,300 m for cones in Ulysses Colles (Brož and Hauber, 2012). Since the area of particle deposition increases with the square of the ballistic range, the total volume of material needed to build a steep cone with flank slopes reaching the angle of repose would have to be significantly (about two orders of magnitude) larger on Mars than on Earth. Considering this, it is not surprising that the scoria cones on Mars are less steep than on Earth and their slopes remain below the angle of repose (Fig. 5.2).

In Fig. 5.4, we compare the shapes of three scoria cones observed in Ulysses Colles (red and orange lines) with those predicted numerically for the wide ejection cone (ECW), a particle size of 4 cm and different ejection velocity distributions (plotted in black). If the particles are ejected with a similar initial velocity as on Earth (mean velocity of 46 m/s), the resulting cone is steeper and has a smaller W_{CO} than actually observed on Mars. However, if we increase the ejection velocity by a factor of about two (cf. Wilson and Head, 1994; Fagents and Wilson, 1996), we obtain a cone which is similar in shape to the observation and whose slope never exceeds the angle of repose.

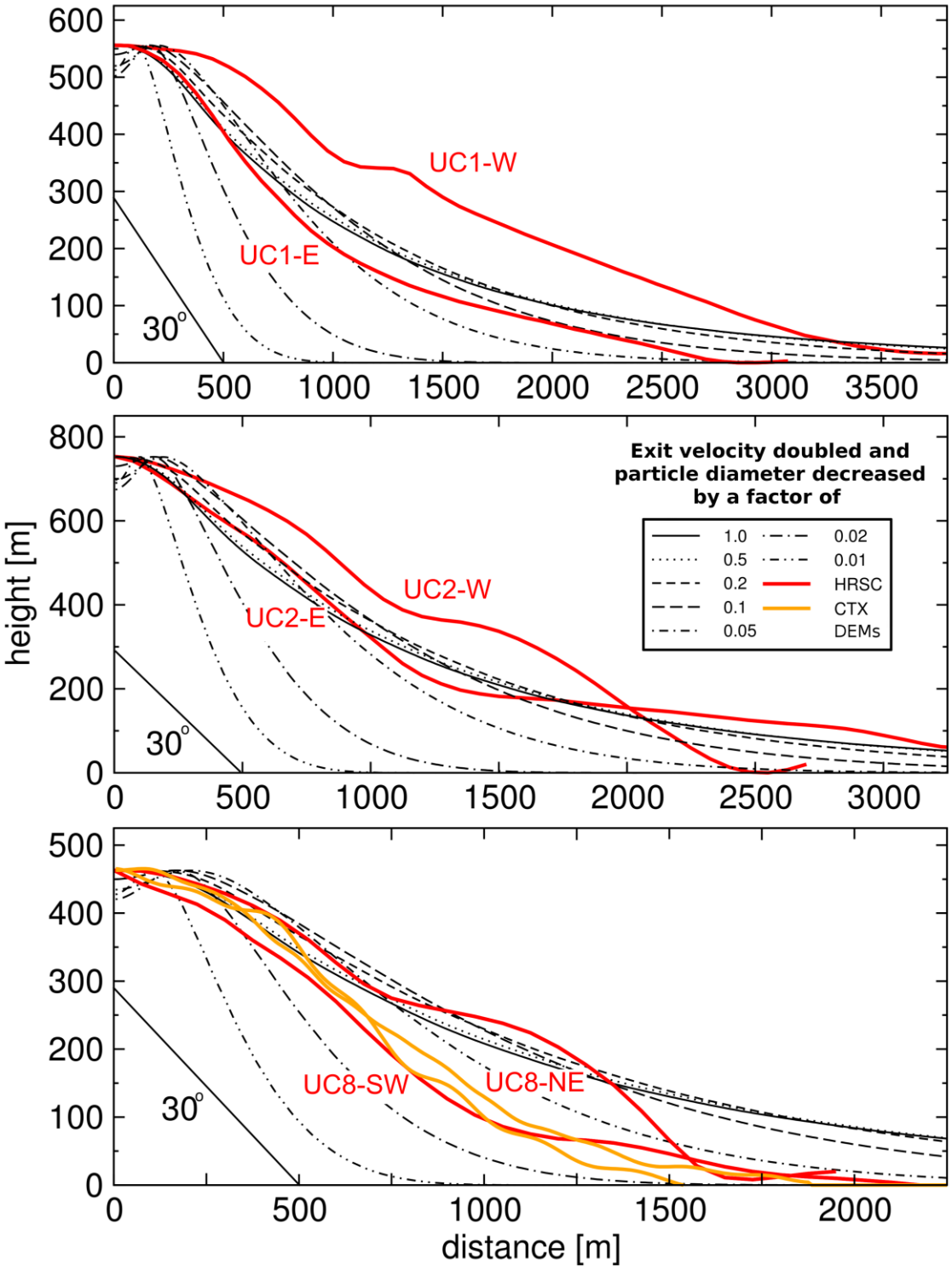

Figure 5.5: The same as in Fig. 5.4 but the model cones (black lines) are computed for two times larger initial velocity than on Earth and various particle-size distributions. The solid black line corresponds to the particle-size distribution as known from Earth while various dashed lines show the cones predicted for particles smaller by a factor of 2, 5, 10, 20, 50, and 100.

The shape of the cone is controlled not only by the initial velocities of ejected particles but also by the distribution of the particle size. In Figure 5.5, we consider an initial velocity which is increased by a factor of two in comparison with the reference model and we test different particle-size distributions in which the particle size is decreased by a factor between 1 and 100. As in Fig. 5.4, the calculation is carried out for the ECW model of ejection angles. When the particles are smaller by a factor of 100, they are deposited in the close vicinity of the vent, forming a cone with slope exceeding 30°. A similar result, though with a somewhat broader W_{CO}, is obtained for particles that are 50 times smaller than in the reference model. Particles that are smaller by a factor of 20, 10 (a factor predicted by Wilson and Head, 1994) and 5, travel further from the vent than finer particles and reach distances which are roughly in agreement with the observation. They are emplaced over a wider area forming a cone where the angle of repose is not reached. A reasonable fit to the observations is also obtained for the particle sizes that are similar as or only slightly (by a factor of 2) smaller than on Earth. However, since the ballistic range of such particles is larger than in the previous case, the agreement between prediction and observation may be deteriorated in the distal zone (see the bottom panel in Fig. 5.5).

The sensitivity of the predicted topographies on particle size and ejection velocity, demonstrated in Figs. 5.4 and 5.5, motivated us to determine those values of these two parameters that yield the best fit of the predicted cone to the observation. We use the standard formulation of the inverse problem, based on the least-squares minimization of the misfit between predicted and observed data,

$$S^2 = \frac{1}{R}\int_0^R \left[h^{obs}(r) - h_{v,d}^{pred}(r)\right]^2 dr \qquad (5.5)$$

where h^{obs} is the averaged topography of the cone, $h_{v,d}^{pred}$ is the topography predicted for ejection velocity v and particle size d, both characterized by a log-normal distribution (see

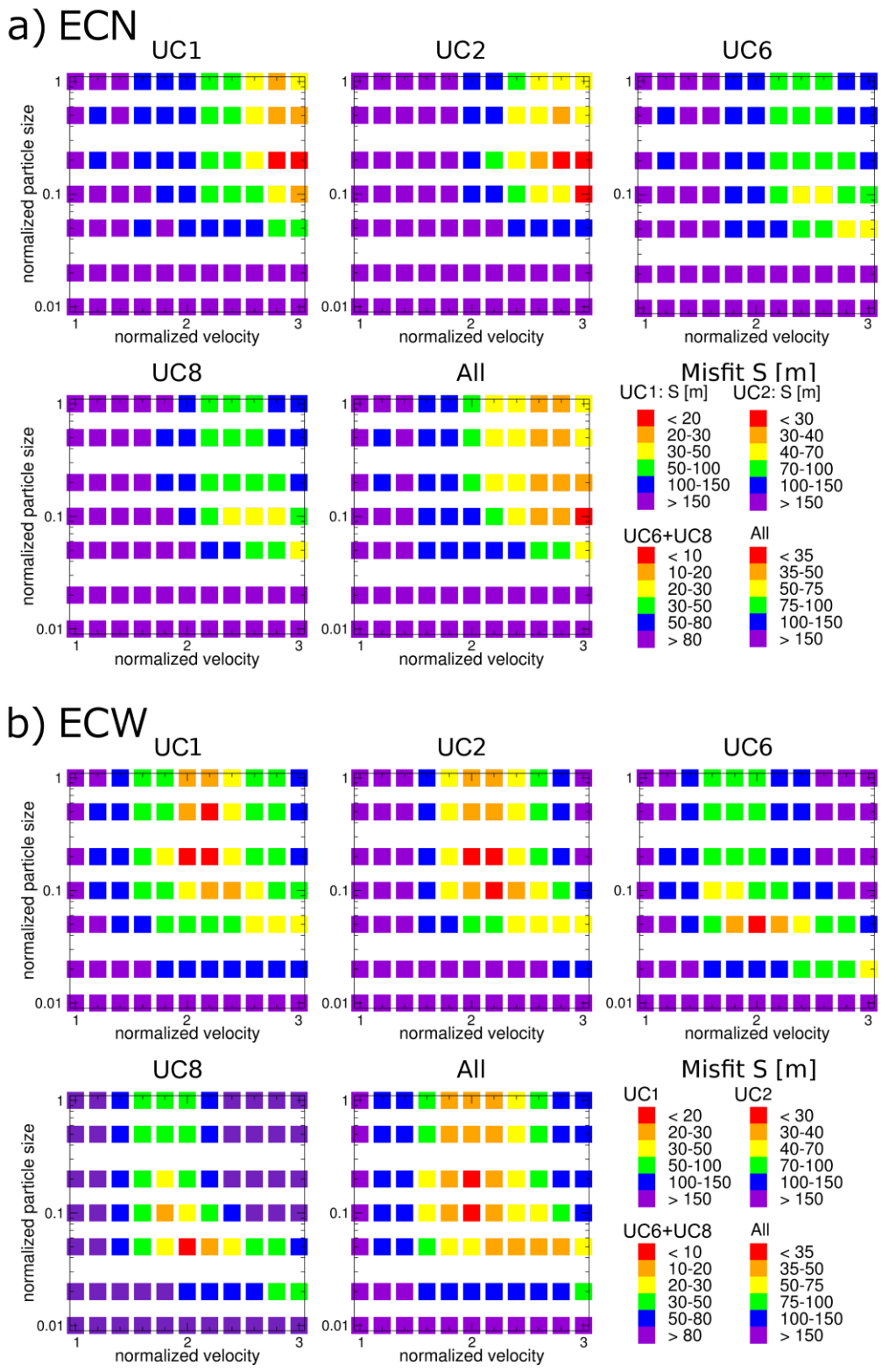

Figure 5.6: Misfit S, eq. (5.5), as a function of normalized ejection velocity and particle size evaluated for ejection angle distributions ECN and ECW. Panel UC1, UC 2, UC 6 and UC 8 show the results obtained for individual scoria cones in Ulysses Colles, panel "All" comprises all available data. The best agreement with observation (red squares) is reached for ejection velocity that is at least 2 larger than on Earth while the best-fitting particle size ranges between 0.05 and 0.5 of the terrestrial value.

section 5.2.1.), and *R* denotes the horizontal extent of the observed cone. The minimum value of *S* is found separately for each of scoria cones UC1, UC2, UC6 and UC8 by a systematic exploration of the parameter space. The results of the inversion are shown in Fig. 5.6 where the misfit *S* is plotted as a function of normalized ejection velocity and particle size separately for the narrow (ECN) and wide (ECW) ejection cone. Note that the agreement between prediction and observation is especially good for cones UC6 and UC8 in the ESW set-up where the best-fitting predicted topography differs from the observed one by less than 10 m in average. In all cases considered, the best fit to observation is found for velocities that are at least about two times larger than on Earth. The optimum value of the normalized particle size ranges between 0.05 (cones UC6 and UC8) and 0.2 (cones UC1 and UC2). When all available data are included (Fig. 5.6, panel 'All'), the preferred value of the normalized particle size is between 0.1 and 0.2, corresponding to a real particle size between 4 and 8 mm. Note that the optimum particle size obtained from the inversion is the same for both ejection angle distributions considered. The choice of parameter $\underline{\sigma_\alpha}$ in eq. (5.3) thus only affects the resultant ejection velocities which are larger for the narrow ejection cone.

Figure 5.7 shows the numerical simulation of a gradual growth of a scoria cone until the instant when the slope of the flank exceeds an angle of 30˚. The simulation of the cone on Earth (top panel, calculated for model ECN) is carried out for the reference values of parameters *d* and *v* while for Mars (bottom panel, calculated for ECW) the values that best predict the shape of cone UC8 are considered. For the modeled terrestrial cones, the angle of 30˚ is attained after deposition of about 0.00084 km^3 of clastic material when the cone is ~40 m high. In contrast, more than 2.17 km^3 of material, corresponding to a height of about 600 m, are needed for the cone on Mars to reach the angle of repose. Such an amount of material was not available on Mars as indicated by comparison of our model with the observed shape of cone UC8 (plotted in red).

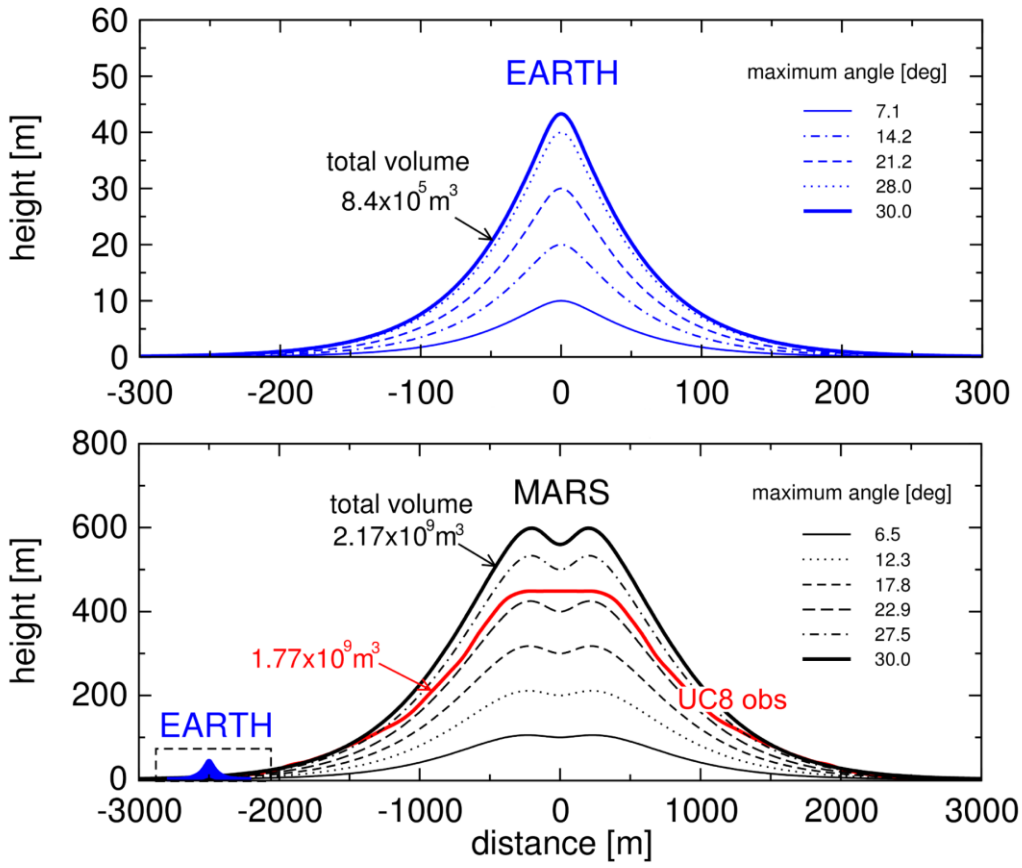

Figure 5.7: Evolution of scoria cones on Earth (top) and Mars (bottom) until the angle of repose (30˚) is reached. The cones are predicted for the reference model and the best-fitting parameters obtained for cone UC8 (Fig. 5.6), respectively. Dashed lines illustrate the gradual growth of the cone. The maximum angle attained for each profile is given in the legend. On Earth, the angle of repose is reached (blue solid line) when the cone is around ~40-m high and its volume is about 8.4×10^5 m^3. The critical height of a cone on Mars (black solid line) is ~600 m, and the angle of repose is reached when the volume of deposited material is about 2.17×10^9 m^3, thus four orders of magnitude larger than typical on Earth. The red profile shows the average topography of scoria cone UC8 based on CTX DEM. Note that the vertical scales are significantly magnified relative to the horizontal scales.

5.4. Discussion

5.4.1. Interpretation of the results

As shown in Fig. 5.3, the area of dispersal increases significantly in martian environmental conditions, and the total volume required to achieve the angle of repose over the entire flank of the cone increases as well. This modeling result explains the different shapes of scoria cones on Mars and Earth. If the typical terrestrial amount of tephra is spread

over a wider area on Mars, the resulting cone has a different morphology from that on Earth, simply because there is less material available in the close vicinity of vent. The outcome will be an edifice with gentler flank slopes and a low topographic profile (Fig. 5.7). Therefore, more material needs to be erupted to build a cone with flank slopes that are dominated by avalanching.

If the cones of Ulysses Colles (Brož and Hauber, 2012) and morphologically similar cones in Hydraotes Chaos (0.07°N; 326.19°E; Meresse et al., 2008) represent typical or average-sized pyroclastic cones on Mars, monogenetic explosive volcanism is more voluminous on Mars than on Earth. For example, cone UC2 in Ulysses Colles has a height of ~650 m and basal diameter of 3,200 m with flank slope of ~27.5°, therefore its total volume is around 2.25 km^3 (Brož and Hauber, 2012). This is at least two orders of magnitude more than the average volume of terrestrial scoria cones (0.046 km^3, determined from 986 edifices, data from Pike, 1978 and Hasenaka and Carmichael, 1985). Much more material reached the surface during explosive eruptions and more voluminous scoria cones were created on Mars as compared with Earth. One possible explanation is that the lower acceleration due to gravity on Mars enables the formation and ascent of larger magma bodies into the crust, and also the formation of wider feeder dikes (Wilson and Head, 1994). On the other hand, if the average volume of explosively erupted material on Mars was smaller, and the observed edifices in Ulysses Colles and Hydraotes Chaos have atypically large volumes, smaller scoria cones must have been formed, too. Their identification in remote sensing data may be complicated, either due to degradational processes or due to their low topographic profiles and gently sloping flanks (as visible on Fig. 5.7).

The growth of cones is initially controlled by the ejection velocities and the deposition mechanism of particles, until the amount of material is critical on the flanks and reaches the static angle of repose. If the angle of repose is reached, future growth is controlled

by particle avalanching, and the shape of the cone cannot be used for ballistic pathway modeling any more (Riedel et al., 2003). The critical value for tephra composing terrestrial scoria cones was established to be ~26.4° for the case of pristine scoria cones (Porter, 1972; Hooper and Sheridan, 1998), with the slope angle mean maximum reaching 29.7°±4.2° (Hooper and Sheridan, 1998). However, the slope angle of flanks is partly dependent on the sizes of particles (Wood, 1980a) and on the amount of spatter material, especially around the top of a cone (Porter, 1972). Therefore a value of 30° to 33° is often used as a characteristic angle of repose (Riedel et al., 2003). It needs to be emphasized again that these values are valid for pristine scoria cones, and older and eroded cones display lower flank slopes due to material transport and dispersion (Hooper and Sheridan, 1998).

Our study shows that the static angle of repose causing material avalanching is not reached during martian cone growth over the entire length of flanks (Figs. 5.2 and 5.7). Higher angles might be reached locally in the steepest parts close to the top of the cone. This is a common situation on Earth, where the deposition of spatter leads to a steepening of the flank slopes near the vent (Porter, 1972). However, the accumulation of material per unit area in a given time period is a function of the distance from the vent (i.e. proximal deposition rates are higher than distal ones). Such non-uniform deposition rates cause the formation of a small and relatively steeper conical body around the vent (Fig. 5.7). As the eruption continues, more material is deposited and a situation might occur where a small cone near the vent reaches the angle of repose and redeposition of the material by avalanching takes place. On Earth, the ballistically-dominated cone is covered by the newly formed cone dominated by avalanching rather soon, because material is ejected only few dozen meters from the vent (Figs. 5.3 and 5.7, see also McGetchin et al., 1974). On the other hand, this is not the case on Mars because material is spread over a much larger area. Hence, the cone dominated by avalanching does not overlie the entire extent

of the ballistically-dominated cone. It has to be noted that such cones dominated by avalanching might develop in the central areas of martian scoria cones, as suggested by the part of profile of the cone UC2 in Fig. 5.4.

Due to a lack of information on flank slopes, it had not previously been recognized that martian scoria cones do not reach the critical angle of repose along their entire length of flanks. The shapes of the cones, therefore, preserve information about explosive eruption processes (initial velocities of ejected particles and their sizes as demonstrated in Fig. 5.6), which can be reconstructed by numerical modeling of ballistic pathways (Fig. 5.4). In turn, if ejection velocities and clast sizes are given or assumed, the distribution of ballistically transported clasts may be used to constrain the atmospheric paleo-pressure at the time of the eruption (Carey and Sparks, 1986, and references therein). The latter approach was applied by Manga et al. (2012) in their study of a volcanic bomb in the Home Plate outcrop in Gusev Crater. The model presented here may also be applied to other terrestrial bodies where results of explosive volcanism were described, for example to volcanic fields containing scoria cones in the Marius Hills on the Moon (Lawrence et al., 2013).

5.4.2. Limitations of the numerical model

As already discussed in section 2.1, our numerical model is deliberately simplified to allow efficient exploration of the parameter space. Before we proceeded to modeling the martian cones we carefully examined the relative importance of individual parameters in our ballistic model. By performing a number of numerical tests (not shown here), we found that the shape of the predicted cone is mainly determined by statistical distributions of ejection angle, initial velocity and particle size. The statistical distribution of ejection angles on Mars is not known. To assess the effect of the ejection angle distribution on the shape of the predicted scoria cone, we consider two models of ejection angles showing a Gaussian distribution. The first one roughly corresponds to the ejection cones observed

on the Earth (Gouhier and Donnadieu, 2010) while the other one assumes a two-times wider distribution of ejection angles than on Earth (cf. Glaze and Bologa, 2000; Wilson and Head, 2007). As shown in Fig. 5.6, both these distributions rather well predict the observed shapes of the scoria cones in the Ulysses Colles region and give the same estimates of the particle size. The only difference is that the narrow ejection cone prefers somewhat higher ejection velocities (factor of 2.4-3.0 larger than on Earth) in comparison with the case when the wide ejection cone is considered (factor of ~2).

In our model, the ejection velocity is considered independent of the particle size. Thi choice is motivated by recent findings by Harris et al. (2012), see also discussion in section 2.1, and indirectly justified by our numerical tests which gave unsatisfactory results if the traditional relationship between ejection velocity and particle size (Steinberg and Babenko, 1978) was considered.

We assume that the ejection velocity and particle size have log-normal distributions. The scale parameters (σ in eq. 5.2) of these distributions are estimated from the data published in Harris et al. (2012) and they are not varied in our parametric study. We admit that the value of parameter σ, if significantly changed, can influence the prediction of the cone shape. In contrast, variations of the drag coefficient are of minor importance provided that its value ranges in a similar manner as on Earth. Our numerical tests also suggest that, to a first approximation, we can neglect the effect of drag reduction near the vent, variations of the atmospheric drag along the ballistic path as well as the dependence of the storage coefficient, eq. (5.4), on the local particle-size statistics. The results of our inversion (Fig. 5.6) prefer the models with high ejection velocities where the radius of the drag reduction zone is small in comparison with the horizontal size of the volcano. We note, however, that the drag reduction would be more important for less-energetic explosions that eject particles with small velocities, because the neglected zone would then be a larger fraction of the total clast range.

Another effect which is not considered in our study is the possible interaction between particles during the flight. If collisions between particles are very frequent, the deposition distance cannot be used to estimate the initial parameters of volcanic eruptions (Tsunematsu et al., 2014). Vanderkluysen et al. (2012) observed on Stromboli that only 12% of the analyzed trajectories of particles showed evidence of collisions. If the percentage of the particles affected by collisions were similar on Mars and Earth, and the particles were distributed more or less randomly over a sufficiently large area, then the effect of collisions would be of only minor importance.

Although it is widely assumed that scoria cones are formed by ballistic emplacement of material around the vent (McGetchin et al., 1974; Parfitt and Wilson, 2008), observations suggest that the reality is more complex (Calvari and Pinkerton, 2004; Valentine et al., 2005; Vanderkluysen et al., 2012). Fire fountaining and deposition of material from ash jets can participate in the formation of scoria cones (Riedel et al., 2003; Calvari and Pinkerton, 2004; Valentine et al., 2005). The majority of particles transported by fire fountaining follow ballistic trajectories, because their large size enables decoupling from the motion of the gases (Carey and Bursik, 2000, p. 531), hence their behavior can be predicted by a ballistic emplacement model. The jet deposition is characterized by non-ballistic movement via turbulent currents potentially introducing a degree of uncertainty in our model. On the other hand, the jet deposition is mainly responsible for a thin ash blanket widely extending beyond the cone itself (Riedel et al., 2003) and, therefore, does not significantly affect the resulting cone's topography. The thin ash blanket would be difficult to detect on topographic profiles based on remote sensing data because it smoothly transitions into surrounding plains. In this study, the boundaries of the cones have been determined on the basis of images accompanied by topographic profiles, where a transition to the surrounding

plains was visible as a break in slope. Therefore, the investigated scoria cones represent clearly detectable landforms where ballistic emplacement dominates over jet deposition.

Scoria cones on Earth are susceptible to rapid erosion, which changes their morphometric characteristics (Wood, 1980b; Dohrenwend et al., 1986; Hooper and Sheridan, 1998). For example, erosion can decrease the flank slopes of scoria cones with a rate of $0.006°/10^3$ yr (Dohrenwend et al., 1986). On Mars, however, the environmental conditions and consequently, the erosion rates are substantially different. Erosion rates on Mars are extremely low after the end of the Noachian (~3.7 Ga) when liquid water became less abundant on the martian surface. For example, Golombek et al. (2006) estimate that the erosion rates in the Amazonian are as low as 1-10 nm/yr. Since the Ulysses Colles scoria cones are much younger than Noachian-aged and formed sometimes between ~1.5 Ga and ~0.44 Ga (Brož and Hauber, 2012), the cumulative erosion since then should not have significantly affected their shape. In fact, there are no traces of erosion visible on their flanks, e.g., rilles or gullies. Moreover, the Ulysses Colles are mantled by a thick layer of dust, which is further evidence that, least at present, aggradational processes dominate over degradational (erosional) processes in this region. Hence, we consider the possible effect of erosion on the slope angles of the studied scoria cones on Mars to be negligible.

5.5. Conclusions

The flank slopes of scoria cones in the Ulysses Colles region on Mars do not reach the critical angle of repose, in contrast to terrestrial scoria cones. Although the volume of the ejected material is much larger than on Earth, it is not sufficient for the critical angle to be reached since it is dispersed over a much larger area during an explosive eruption. Because the cones on Mars did not reach the angle of repose, their morphological shape still preserves a record of environmental conditions at the time of eruption. This suggests that

numerical modeling could be used to examine in more detail the basic physical parameters controlling cone formation and hence refine earlier theoretical predictions. Our results show that to build a scoria cone on Mars as observed, the initial velocity of ejected particles has to be increased by a factor of at least ~2 with respect to the typical velocity on Earth, corresponding to a mean particle velocity of ~92 m/s or higher, and that the particles have to be finer by a factor of 0.1 and 0.2, corresponding to a real particle size of 4 to 8 mm. Our findings thus confirm earlier theoretical predictions by Wilson and Head (1994) and help us to understand the development of scoria cones on Mars. A similar approach might be used on other terrestrial bodies from which small-scale volcanoes of explosive origin were reported.

Acknowledgements

We thank M.G. Kleinhans who kindly provided the data for values of angle of repose, J. L. Grenfell who informed us about dependence of atmospheric pressure on altitude, Matt Balme for helpful discussions, A. Clarke for her constructive comments on a previous version of this manuscript, and an anonymous reviewer for his inspiring suggestions. PB is thankful to Václav Kuna for help to refine the initial idea. Hetu Sheth kindly provided the image shown in Fig. 5.2b, and Tim Jonas helped with LIDAR data to create Fig. 5.2c. This study was supported by the Grant No. 580313 from the Grant Agency of Charles University in Prague (GAUK) and by the Helmholtz Association through the research alliance 'Planetary Evolution and Life'.

References

Alatorre-Ibargüengoitia, M. A., Delgado-Granados, H., 2006. Experimental determination of drag coefficient for volcanic materials: Calibration and application of a model to Popocatépetl volcano (Mexico) ballistic projectiles, Geophysical Research Letters, vol. 33, L11302, doi: 10.1029/2006GL026195.

Atwood-Stone, C., McEwen, A.S., 2013. Avalanche Slope Angles in Low Gravity Environments from Active Martian Sand Dunes, Geophysical Research Letters, doi: 10.1002/grl.50586.

Bird, R.B., Steward, W.E., Lightfood, E.N., 1960. Transport Phenomena, John Wiley and Sons, New York.

Bleacher, J.E., Greeley, R., Williams, D.A., Cave, S.R., Neukum, G., 2007. Trends in effusive style at the Tharsis Montes, Mars, and implications for the development of the Tharsis province, J. Geophys. Res., 112, E09005, doi:10.1029/2006JE002873.

Brož, P., Hauber, E., 2012. An unique volcanic field in Tharsis, Mars: Pyroclastic cones as evidence for explosive eruptions, Icarus, 218, 1, 88–99, doi:10.1016/j.icarus.2011.11.030.

Brož, P., Hauber, E., 2013. Hydrovolcanic tuff rings and cones as indicators for phreatomagmatic explosive eruptions on Mars, J. Geophys. Res., 118, 1656-1675, doi: 10.1002/jgre.20120.

Calvari, S., Pinkerton, H., 2004. Birth, growth and morphologic evolution of the ‘Laghetto’ cinder cone during the 2001 Etna eruption, Journal of Volcanology and Geothermal Research 132 (2004) 225-239, doi:10.1016/S0377-0273(03)00347-0.

Carey, S., Sparks, R.S.J., 1986. Quantitative models of the fallout and dispersal of tephra from volcanic eruption columns, Bulletin of Volcanology 48, 109–125, doi: 10.1007/BF01046546.

Carey, S., Bursik, M. 1999. Volcanic plumes, in Encyclopedia of volcanoes, edited by H. Sigurdsson, pp. 527–544, Academic Press, San Diego, California.

Dehn, J., Sheridan, M.F., 1990. Cinder cones on the Earth, Moon, Mars, and Venus: A computer model, Lunar Planet. Sci. XXI, 270 (abstract).

Dohrenwend, J. C., Wells, S. G., Turrin, B. D., 1986. Degradation of Quaternary cinder cones in the Cima volcanic field, Mojave Desert, California. Geol. Soc. Am. Bull. 97, 421–427.

Fagents, S.A., Wilson, L., 1993. Explosive volcanic eruptions—VII. The ranges of pyroclasts ejected in transient volcanic explosions, Geophys. J. Int., 113(2), 359-370, doi:10.1111/j.1365-246X.1993.tb00892.x.

Fagents, S.A., Wilson, L., 1996. Numerical modeling of ejecta dispersal from transient volcanic explosions on Mars, Icarus 123, 284–295, doi: 10.1006/icar.1996.0158.

Glaze, L. S., Baloga, S. M., 2000, Stochastic-ballistic eruption plumes on Io. Journal of Geophysical Research: Planets 105, 17579–17588, doi: 10.1029/1999JE001235.

Golombek, M. P., et al., 2006. Erosion rates at the Mars Exploration Rover landing sites and long-term climate change on Mars. J. Geophys. Res. 111, E12S10, doi: 10.1029/2006JE002754.

Gouhier M., Donnadieu, F., 2010. The geometry of Strombolian explosions: insights from Doppler radar measurements, Geophys. J. Int., 183, 1376–1391, doi: 10.1111/j.1365-246X.2010.04829.x.

Gwinner, K., Scholten, F., Preusker, F., Elgner, S., Roatsch, T., Spiegel, M., Schmidt, R., Oberst, J., Jaumann, R., Heipke, C., 2009. Topography of Mars from global mapping by HRSC high-resolution digital terrain 2 models and orthoimages: Characteristics and performance, Earth Planet. Sci. Lett., 294, 506–519, doi:10.1016/j.epsl.2009.11.007.

Harris, A.J.L, Ripepe, M., Hughes, E.A., 2012. Detailed analysis of particle launch velocities, size distributions and gas densities during normal explosions at Stromboli, J. Volcanol. Geotherm. Res., doi:10.1016/j.jvolgeores.2012.02.012.

Hasenaka, T., Carmichael, I.S.E., 1985. The cinder cones of Michoacán–Guanajuato, central Mexico: Their age, volume and distribution, and magma discharge rate. J. Volcanol. Geotherm. Res. 25, 104–124.

Hooper, D.M., Sheridan, M.F., 1998. Computer-simulation models of scoria cone degradation, J. Volcanol. Geotherm. Res. 83, 241–267, doi: 10.1016/S0377-0273(98)00031-6.

Jaumann, R., et al., 2007. The high-resolution stereo camera (HRSC) experiment on Mars Express: Instrument aspects and experiment conduct from interplanetary cruise through the nominal mission, Planet. Space Sci., 55, 928–952, doi: 10.1016/j.pss.2006.12.003.

Jaupart, C., Vergniolle, S., 1989. The generation and collapse of a foam layer at the roof of a basaltic magma chamber, J. Fluid Mech., 203, 347–380, doi: 10.1017/S0022112089001497.

Kerber, L., Forget, F., Madeleine, J.-B., Wordsworth, R., Head, J. W., Wilson, L., 2013. The effect of atmospheric pressure on the dispersal of pyroclasts from martian volcanoes, Icarus, 223, 1, 149–156, doi:10.1016/j.icarus.2012.11.037.

Keszthelyi, L. et al., 2008. High Resolution Imaging Science Experiment (HiRISE) images of volcanic terrains from the first 6 months of the Mars Reconnaissance Orbiter primary science phase, J. Geophys. Res. 113, E04005, doi:10.1029/ 2007JE002968.

Kleinhans, M.G., Markies, H., de Vet, S. J., in 't Veld, A. C., Postema, F. N., 2011. Static and dynamic angles of repose in loose granular materials under reduced gravity, J. Geophys. Res. 116, E11004, doi:10.1029/2011JE003865.

Lawrence, S. J., et al., 2013. LRO observations of morphology and surface roughness of volcanic cones and lobate lava flows in the Marius Hills, J. Geophys. Res. Planets, 118, doi:10.1002/jgre.20060.

Lautze, N.C., Houghton, B.F., 2005. Physical mingling of magma and complex eruption dynamics in the shallow conduit at Stromboli volcano, Italy. Geology 33 (5), 425–428.

Malin, M. C., et al., 2007. Context camera investigation on board the Mars Reconnaissance Orbiter, J. Geophys. Res., 112, E05S04, doi:10.1029/2006JE002808.

Manga, M., Patel, A., Dufek, J., Kite, E. S., 2012. Wet surface and dense atmosphere on early Mars suggested by the bomb sag at Home Plate, Mars, Geophys. Res. Lett., 39, L01202, doi:10.1029/2011GL050192.

McGetchin, T.R., M. Settle, and B.A. Chouet, 1974, Cinder cone growth modelled after North East crater, Mt Etna, Sicily, J. Geophys. Res. 79, 3257-3272, doi: 10.1029/JB079i023p03257.

Meresse, S., Costard, F., Mangold, N., Masson, P., Neukum, G., the HRSC Co-I Team, 2008. Formation and evolution of the chaotic terrains by subsidence and magmatism: Hydraotes Chaos, Mars, Icarus 194, 487–500, doi: 10.1016/j.icarus.2007.10.023.

Moratto, Z.M., Broxton, M.J., Beyer, R.A., Lundy, M., Husmann K., 2010. Ames Stereo Pipeline, NASA's Open Source Automated Stereogrammetry Software. In: 41st Lunar and Planetary Institute Science Conference, Houston, Texas [2364].

Parfitt, E.A., Wilson, L., 2008. Fundamentals of Physical Volcanology, Blackwell, Oxford, 256pp.

Pike, R.J., 1978. Volcanoes on the inner planets: Some preliminary comparisons of gross topography. Proc. Lunar Sci. Conf. IX, 3239–3273.

Porter, S.C., 1972. Distribution, morphology, and size frequency of cinder cones on Mauna Kea Volcano, Hawaii, Bull. Geol. Soc. Am. 83, 3607–3612, doi: 10.1130/0016-7606(1972)83[3607:DMASFO]2.0.CO;2.

Riedel, C., Ernst, G.G.J., Riley, M., 2003. Controls on the growth and geometry of pyroclastic constructs, J. Volcanol. Geotherm. Res. 127, 121–152, doi: 10.1016/S0377-0273(03)00196-3.

Saunderson, H.C., 2008. Equations of motion and ballistic paths of volcanic ejecta, Computational Geosciences 34, 802–814, doi: 10.1016/j.cageo.2007.10.004.

Steinberg, G.S., Babenko, J.L., 1978. Gas velocity and density determination by filming gas discharges, Journal of Volcanology and Geothermal Research 3, 89–98.

Tsunematsu K., Chopard, B., Falcone, J.-L., Bonadonna, C., 2014. A numerical model of ballistic transport with collisions in a volcanic setting, Computers & Geosciences, Volume 63, 62-69, 10.1016/j.cageo.2013.10.016.

Valentine, G. A., Kier, D., Perry, F. V., Heiken, G., 2005. Scoria cone construction mechanisms, Lathrop Wells volcano, southern Nevada, USA, Geology 33, 629-632, doi: 10.1130/G21459AR.1.

Vanderkluysen, L., Harris, A.J.L., Kelfoun, K., Bonadonna, C., Ripepe, M., 2012. Bombs behaving badly: unexpected trajectories and cooling of volcanic projectiles. Bullet. Volcanol. 74 (8), 10.1007/s00445-012-0635-8.

Wilson, L., Head, J. W., 1994. Review and analysis of volcanic eruption theory and relationships to observed landforms, Rev. Geophys. 32, 221–263, doi:10.1029/94RG01113.

Wilson, L., Head, J.W., 2007. Explosive volcanic eruptions on Mars: tephra and accretionary lapilli formation, dispersal and recognition in the geological record. J. Volcanol. Geotherm. Res. 163, 83–97, doi: 10.1016/j.jvolgeores.2007.03.007.

Wood, C.A., 1979. Cinder cones on Earth, Moon and Mars, Lunar Planet. Sci. X, 1370–1372 (abstract).

Wood, C.A., 1980a. Morphometric evolution of cinder cones, J. Volcanol. Geotherm. Res. 7, 387–413.

Wood, C. A., 1980b. Morphometric analysis of cinder cone degradation. J. Volcanol. Geotherm. Res. 8, 137–160.